

Stereodynamics of the vibrational channel $O(1D) + H_2O \rightarrow OH(v'=2) + OH$

Hiroshi Tsurumaki, Yo Fujimura, and Okitsugu Kajimoto

Citation: *The Journal of Chemical Physics* **110**, 7707 (1999); doi: 10.1063/1.478682

View online: <http://dx.doi.org/10.1063/1.478682>

View Table of Contents: <http://scitation.aip.org/content/aip/journal/jcp/110/16?ver=pdfcov>

Published by the [AIP Publishing](#)

Articles you may be interested in

[Relaxation of \$H_2O\$ from its \$J_04\$ – vibrational state in collisions with \$H_2O\$, Ar, \$H_2\$, \$N_2\$, and \$O_2\$](#)

J. Chem. Phys. **120**, 5592 (2004); 10.1063/1.1649726

[The branching ratio between reaction and relaxation in the removal of \$H_2O\$ from its \$J_04\$ – vibrational state in collisions with H atoms](#)

J. Chem. Phys. **115**, 4586 (2001); 10.1063/1.1389304

[The dynamics of the reactions \$H+H_2O \rightarrow OH+H_2\$ and \$H+D_2O \rightarrow OD+HD\$ at 1.4 eV](#)

J. Chem. Phys. **114**, 6690 (2001); 10.1063/1.1356008

[The product rovibrational and spin–orbit state dependent dynamics of the complex reaction \$H+CO_2 \rightarrow OH\(2 \Pi; v, N, \Omega, f\) + CO\$: Memories of a lifetime](#)

J. Chem. Phys. **112**, 4557 (2000); 10.1063/1.481081

[Translational to vibrational and rotational \(\$T \rightarrow V, R\$ \) energy transfer and reactive exchange collisions of \$H\(D\) + HF\(DF\)\$ in the energy range from 1 to 2 eV by time-resolved Fourier transform spectroscopy](#)

J. Chem. Phys. **106**, 2265 (1997); 10.1063/1.473149



Stereodynamics of the vibrational channel $O(^1D) + H_2O \rightarrow OH(v' = 2) + OH$

Hiroshi Tsurumaki, Yo Fujimura, and Okitsugu Kajimoto

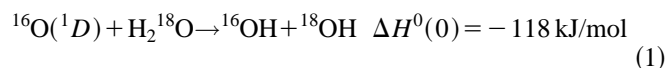
Department of Chemistry, Graduate School of Science, Kyoto University, Kitashirakawa-Oiwakecho, Sakyo-ku, Kyoto 606-8502, Japan

(Received 30 October 1998; accepted 25 January 1999)

The state-selected differential cross section (DCS) and rotational angular momentum polarization for the reaction $O(^1D) + H_2O \rightarrow OH + OH$ have been measured by utilizing the polarized Doppler-resolved laser-induced fluorescence probing technique. Stereodynamics of the reaction channel forming the newly formed OH in the specific vibrational level $v' = 2$ is discussed on the basis of the vector properties. A nearly isotropic DCS for the product $OH(^2\Pi_{3/2}, v' = 2, j' = 5.5)$ most probably indicates that the reaction is dominated by an insertion mechanism involving a collisional HOOH complex with a lifetime comparable to its rotational period. The extremely asymmetrical energy partitioning between the two OH fragments, therefore, suggests that the redistribution of the available energy does not occur on a time scale comparable to the rotational period of the complex. Furthermore, it has been found that the product rotational angular momentum vector \mathbf{j}' is predominantly perpendicular to the collision plane spanned by \mathbf{k} and \mathbf{k}' (the relative velocity vectors of the reactants and products, respectively) both for the forward- and backward-scattered products. It suggests that the initially excited bending motion of the H–O–O moiety in the collisional HOOH complex primarily contributes to the product rotation. © 1999 American Institute of Physics. [S0021-9606(99)00816-8]

I. INTRODUCTION

The reaction of electronically excited oxygen atom, $O(^1D)$ with H_2O plays an important role as a source of OH radicals in the stratosphere. The two OH product molecules produced from this reaction are chemically identical but their origins are distinctly different, i.e., “new” OH formed in the reaction and “old” OH present in the H_2O reagent from the beginning. To distinguish these two types of OH products for the detailed analysis of the reaction dynamics, the reaction with isotopically labeled reagent $H_2^{18}O$,



has been studied.^{1–11}

Pioneering measurements using the $H_2^{18}O$ reagents in early 1980s, revealed that the newly formed ^{16}OH is vibrationally and rotationally much more excited than the old ^{18}OH .^{1–4} This unequal energy partitioning was explained by a direct process such as abstraction or stripping.

About 10 years later, with the development of the detection technique of laser-induced fluorescence (LIF), the titled reaction was reexamined under collision-free conditions^{5,6} which were not achieved in the earlier experiments.^{1–4} The new experiments free from the rotational relaxation of the nascent products showed remarkable rotational excitation of the new OH compared with the old OH. In addition, the Λ -doublet state distribution measured in these studies showed some preferential formation of the $\Pi(A')$ component. Based on these observation, Cleveland *et al.* proposed a direct insertion mechanism with a collisional HOOH com-

plex breaking up prior to the redistribution of the available energy among its internal modes.⁵

To determine whether the reaction proceeds via direct abstraction, stripping or insertion pathways, the measurement of product differential cross section (DCS) is most desirable. Along this line, King *et al.* measured the LAB frame speeds of both the new and old OH products by utilizing polarized Doppler spectroscopy.⁷ They fit the Doppler profiles representing the product LAB speed distribution with a single parameter of average LAB kinetic energy and estimated a representative average center-of-mass (CM) scattering angle under several assumptions. Their observation of broader linewidth of the new OH than that of the old OH was explained by the strong scattering anisotropy in the CM frame. Based on such analysis, they concluded that the fragmentation of the collision complex proceeds promptly with the lifetime less than 100 fs. The difference of the linewidth between the new and old OH molecules shown by King *et al.* is indeed very obvious. However, it has also been shown that the internal energy content of the new OH is far larger than that of the old OH.^{5,6} Therefore, the difference of the linewidth between the new and old OH molecules can arise from this asymmetric energy partitioning between the two OH products. Thus, the product LAB speed cannot be uniquely related to the CM scattering angle. Consequently, the additional information such as the product LAB recoil anisotropy is required for uniquely determining the product DCS with the translational energy distribution.

In recent years, precise determination of the DCS, translational energy distribution, and polarization of rotational angular momentum of molecular products in bimolecular reactions have been performed by several groups.^{12–31} The

theory to extract such information with the Doppler probing technique has been well established by Aoiz *et al.*^{32,33} With this sophisticated procedure, stereodynamics of several reactions of fundamental importance have been analyzed in detail so far.^{14–22} We have re-examined the titled reaction by using this method. Although the isotopically labeled reaction (1) is essential in distinguishing the two types of OH products, we used the isotopically unlabeled normal H₂O reagents in this study. However, by probing the OH products generated in the specific vibrational level $v'=2$, the newly formed OH can be selectively observed since the previous works reported that the amount of the old OH in $v'=2$ was negligible.^{5,6} We have measured the state-selected DCS and rotational angular momentum polarization of the newly formed OH(²Π_{3/2}, $v'=2$, $j'=5.5$) by utilizing polarized Doppler spectroscopy. The reaction dynamics is discussed on the basis of thus obtained relatively isotropic DCS and the angular correlation of \mathbf{j}' which is perpendicular to the collision plane spanned by \mathbf{k} and \mathbf{k}' , the relative velocity vectors of the reactants and products, respectively. The results suggest an insertion mechanism involving a collisional HOOH complex with the main contribution of H–O–O bending motion to the product OH rotation. Even the HOOH intermediate complex can survive for its rotational period, it breaks up prior to the energy randomization, resulting in the asymmetrical energy partitioning between the two OH fragments.

II. EXPERIMENT

The experimental apparatus is schematically depicted in Fig. 1(a). Experiments were carried out in a stainless steel vacuum chamber. A mixture of N₂O and H₂O vapor was introduced into the reaction chamber and the flow rate was controlled with stainless steel needle valves. Nitrous oxide (Showa Denko, 99.999%) and distilled H₂O were used without further purification. The sample gases in the reaction chamber were continuously pumped by using a rotary pump. The partial pressures of N₂O and H₂O vapor were about 100 and 50 mTorr at 300 K, respectively. The electronically excited oxygen atom, O(¹D) was generated from the photodissociation of N₂O at 193 nm with an ArF excimer laser (Lambda Physik EMG 53MSC). At a time delay of 120 ns after the photolysis laser radiation, a tunable UV light (TMQ, 346–355 nm) of a dye laser (Lambda Physik SCANmate 2E) pumped by a XeCl excimer laser (Lambda Physik COMPex 102) was introduced into the reaction chamber to probe the nascent product OH($v'=2$) by laser-induced fluorescence (LIF) via the OH A ²Σ⁺–X ²Π (1,2) excitation in the spectral region of 348–352 nm. Measurements of Doppler profiles were performed by using the probe laser with an intracavity étalon which yields the bandwidth of about 0.04 cm⁻¹ in full-width at half-maximum (FWHM).

The fluorescence was collected by a synthetic silica lens and focused by another silica lens on a photomultiplier tube (Hamamatsu R928) mounted perpendicular to both of the photolysis and probe laser beam axes. An interference filter (Nippon Sinku Kogaku 6205–5989) centered at 310 nm with 13.5 nm FWHM was placed in front of the photomultiplier tube to transmit only OH A ²Σ⁺–X ²Π (1,1) emission by blocking the strong scattered light and emission arising from

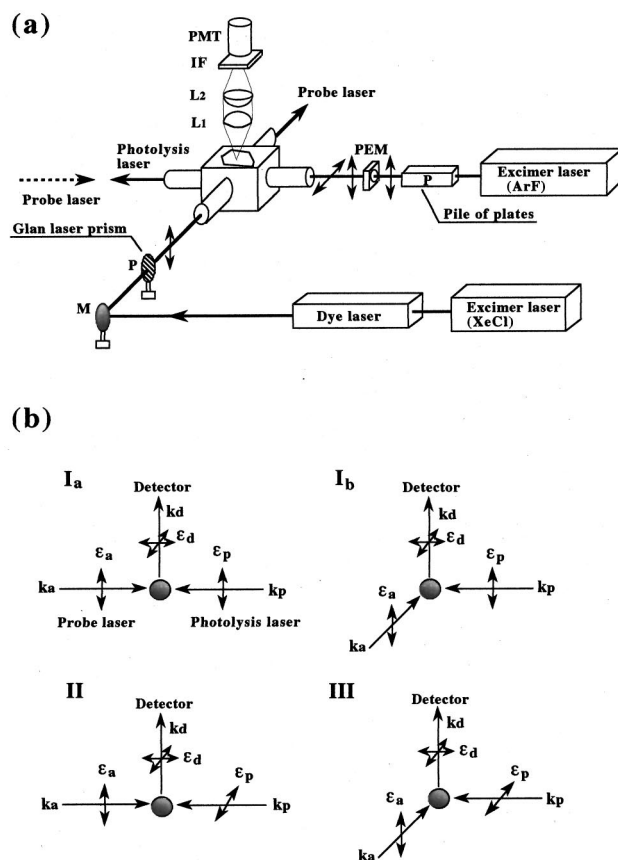


FIG. 1. (a) Schematic diagram of the experimental apparatus used in the measurement of Doppler profiles. *M*, mirror; *P*, polarizer; PEM, photoelastic modulator; *L_i*, synthetic silica lens; IF, interference filter; and PMT, photomultiplier tube. The probe laser beam was introduced into the vacuum chamber either collinearly or orthogonally to the photolysis laser beam. (b) Characterization of the LIF excitation-detection geometries employed in the measurement of Doppler profiles. The vectors of \mathbf{k} and $\boldsymbol{\epsilon}$ represent the propagation and electric vectors of the laser light or fluorescence, respectively. The subscripts *p*, *a*, and *d* imply the photolysis, absorbed, and detected photons, respectively.

the photolysis and probe lasers. Such $\Delta v = -1$ excitation with $\Delta v = 0$ detection was essential to improve the signal to noise ratio. The LIF signal was amplified by a fast preamplifier (Comlinear CLC 100) and gated by a boxcar integrator (Stanford Research System SR 250). The gated signal was digitized by an A/D converter (Stanford Research System SR245) and stored in a personal computer via a GPIB interface. The pump-probe experiments were performed at a repetition rate of 10 Hz. The timing of the laser system was adjusted by a digital pulse/delay generator (Stanford Research System DG 535). Each laser power was monitored by a photodiode (Hamamatsu 1336-5BQ) for normalizing the LIF signal to correct for the fluctuation of the power.

The present experiments utilized the photolysis of N₂O at 193 nm for generating O(¹D). Different from the O₃ photolysis at 266 nm (Refs. 1–4, 6–9) or 248 nm (Ref. 5) so far used, the photolysis at 193 nm could also photolyze H₂O and produce OH fragments.³⁴ Although a very small amount of contamination due to the OH photofragments was observed in $v'=0$, we confirmed that such contamination was abso-

lately negligible in $v' = 2$ as consistent with the extremely cold vibrational distribution of the OH photofragments ($P_{v'=1}/P_{v'=0} < 0.03$) reported by Grunewald *et al.*³⁴

The effect of collisional relaxation was also carefully examined since it has been found that the OH($A^2\Sigma^+$) and OH($X^2\Pi$) are effectively deactivated by the collisions with H₂O.^{5,35} The Doppler line shapes did not show any appreciable changes within experimental errors with varying the total pressure of 2:1 N₂O/H₂O mixed sample gas from 75 mTorr to 150 mTorr at a 120 ns pump–probe delay. Therefore, the deactivation of OH($A^2\Sigma^+$) and OH($X^2\Pi$) is negligible under the experimental conditions employed in the present study. Moreover, we ensured that the probe laser power was weak enough to avoid the saturation effect in the OH $A^2\Sigma^+ - X^2\Pi$ (1,2) transition.

The Doppler-resolved spectral line profiles were measured in the three different LIF excitation-detection geometries I, II, and III shown in Fig. 1(b) according to a combination in the directions of the polarization and propagation vectors of each laser. Incomplete vertical polarization of the output of the probe laser was converted to higher vertical linear polarization (degree of polarization > 0.99) with a Glan laser prism (Meiritsu LAN-10-L). The direction of the polarization vector of the probe laser light denoted as ϵ_a in Fig. 1(b) was always vertical in all the excitation-detection geometries. The originally unpolarized ArF laser light was passed through a pile of plates consisting of twelve Brewster's angle quartz plates to obtain a vertically polarized light (degree of polarization > 0.95). The firing of the ArF laser was synchronized to the stress cycle of a photoelastic modulator (Hinds PEM 90). By changing the arrival timing of the polarized 193 nm light at the photoelastic modulator, one can control the polarization of the light passing through this modulator. The trigger pulses for the shot-by-shot alternation of the two appropriate timings corresponding to the vertical and horizontal polarization were generated with home-made electronic devices. This shot-by-shot alternation of the polarization vector allows us to observe the two polarization-dependent spectral line profiles in the LIF geometries of I_b and III in a single scan. In order to improve the signal to noise ratio, 50–100 laser shots were averaged at each step of a frequency scan and the spectra obtained from 9 to 25 scans were summed up.

Polarization measurements were performed for the rotational transitions of $R_1(5.5)$ and $Q_1(5.5)$. Unfortunately, the signal intensities of their respective associated satellites were too weak to separately probe the dynamics of the two Λ -doublet states. We discuss the adequacy of the analysis using only the main branches of different Λ -doublet states in Sec. IV. The rotational alignment $A_0^{(2)}$ used in the Doppler profile analysis was determined by the ratio of the area of the Doppler profile obtained in the geometry I_b to that obtained in the geometry III at a single scan with the shot-by-shot polarization alternation method described above. The average value over about 25 scans was 0.00 ± 0.03 for both of $R_1(5.5)$ and $Q_1(5.5)$.

III. ANALYSIS

A. Doppler-resolved line profile

In recent years, based on the Dixon's formulation for the Doppler analysis of the vector correlations in photodissociation processes,³⁶ Aoiz *et al.* have developed the theoretical basis to analyze the mutual angular correlations among the LAB velocity vector of the atomic reagent (\mathbf{v}), LAB velocity vector (\mathbf{v}'), and rotational angular momentum vector (\mathbf{j}') of the product molecules in photo-initiated bimolecular reactions from the polarized Doppler-resolved line profiles as described below.^{32,33} In case of the linearly polarized pump-probe experiment, the 1 + 1 LIF Doppler profile $D(\nu)$ as a function of the displaced frequency ν from the line center frequency ν_0 can be written by the Legendre polynomial expansion of $P_n(x)$ up to the second order as

$$D(\nu) = \int_{v_p = |(\nu/\nu_0)c|}^{\infty} \frac{1}{2v'} \left[g_0(v') + g_2(v') P_2\left(\frac{v_p}{v'}\right) \right] dv', \quad (2)$$

where $v_p = |(\nu/\nu_0)c|$ (c , the speed of light) represents the minimum product LAB speed giving the displaced frequency ν as the Doppler shift according to the projection of \mathbf{v}' along the propagation direction of the probe laser, \mathbf{k}_a . The coefficients $g_0(v')$ and $g_2(v')$ in Eq. (2) are expressed as

$$g_0(v') = b_0 \overline{\beta_0^0(0,0;v')} + b_1 \frac{\beta_{\text{photo}}}{2} \overline{\beta_0^2(0,2;v')} \quad (3)$$

and

$$g_2(v') = b_2 \frac{\beta_{\text{photo}}}{2} \overline{\beta_0^2(2,0;v')} + b_3 \overline{\beta_0^0(2,2;v')} + b_4 \frac{\beta_{\text{photo}}}{2} \overline{\beta_0^2(2,2;v')}, \quad (4)$$

where β_{photo} is the translational anisotropy parameter of the atomic reagent produced from the photodissociation of a molecular precursor. The $\overline{\beta_0^K(k_1, k_2; v')}$ represents the bipolar moments averaged over all the possible velocities of the reagents and reflects the vector correlations as a function of product LAB speed v' . The multipliers b_i of bipolar moments in g_0 and g_2 depend on the LIF excitation-detection geometries shown in Fig. 1(b) and the types of rotational transitions. As shown by Docker,³⁷ an appropriate linear combination of the Doppler profiles measured in several LIF geometries for two different types of rotational transitions (P or R vs Q) gives the composite Doppler profile which depends on a single bipolar moment $\overline{\beta_0^K(k_1, k_2; v')}$ in g_0 or g_2 . The composite Doppler profile $D_0^K(k_1, k_2; \nu)$ reflecting each bipolar moment $\overline{\beta_0^K(k_1, k_2; v')}$ is expressed as³³

$$D_0^K(k_1, k_2; \nu) = \int_{v_p = |(\nu/\nu_0)c|}^{\infty} \frac{1}{2v'} \overline{\beta_0^K(k_1, k_2; v')} P_{k_1}\left(\frac{v_p}{v'}\right) dv'. \quad (5)$$

The composite Doppler profiles $D_0^0(0,0;\nu)$ and $D_0^2(2,0;\nu)$ corresponding to the leading terms in g_0 and g_2 are related to the LAB speed distribution (population) and $\mathbf{v}-\mathbf{v}'$ correlation (anisotropy), respectively. The other three composite Doppler profiles reflect the polarization of the product rotational angular momentum vector, \mathbf{j}' ; $D_0^2(0,2;\nu)$ for $\mathbf{v}-\mathbf{j}'$; $D_0^0(2,2;\nu)$ for $\mathbf{v}'-\mathbf{j}'$, and $D_0^2(2,2;\nu)$ for $\mathbf{v}-\mathbf{v}'-\mathbf{j}'$ correlations.

B. Extraction of the product state-selected vector correlations in the CM frame

The vector correlations in the LAB frame represented by $D_0^K(k_1, k_2; \nu)$ need to be transformed into those in the center-of-mass (CM) frame; the angular correlations among the relative velocity vectors of the reactants (\mathbf{k}) and products (\mathbf{k}'), and the product rotational angular momentum vector (\mathbf{j}'). The angular distribution function $P(\omega_t, \omega_r)$ representing the mutual orientation among the three vectors \mathbf{k} , \mathbf{k}' , and \mathbf{j}' is expressed as the expansion in modified spherical harmonics $C_{kq}(\theta_r, \phi_r)$ (Ref. 38) with a set of coefficients $(1/\sigma)d\sigma_{kq}/d\omega_t$ which is defined as polarization-dependent differential cross sections (PDDCSs),³⁹

$$P(\omega_t, \omega_r) = \sum_{k,q} \frac{2k+1}{4\pi} \frac{1}{\sigma} \frac{d\sigma_{kq}}{d\omega_t} C_{kq}(\theta_r, \phi_r)^*, \quad (6)$$

where $\omega_t \equiv (\theta_t, \phi_t)$ and $\omega_r \equiv (\theta_r, \phi_r)$ are the polar and azimuthal angles representing the directions of \mathbf{k}' and \mathbf{j}' , respectively, with respect to \mathbf{k} . Furthermore, the angular distribution function $P(\theta_r, \phi_r)$ representing the product rotational angular momentum polarization with reference to \mathbf{k} and \mathbf{k}' plane is obtained by integrating $P(\omega_t, \omega_r)$ over the whole scattering angles

$$\begin{aligned} P(\theta_r, \phi_r) &= \int P(\omega_t, \omega_r) d\omega_t \\ &= \sum_{k,q} \frac{2k+1}{4\pi} a_{kq} C_{kq}(\theta_r, \phi_r)^*, \end{aligned} \quad (7)$$

where

$$a_{kq} = \int \frac{1}{\sigma} \frac{d\sigma_{kq}}{d\omega_t} d\omega_t. \quad (8)$$

Aoiz *et al.* have shown the relationship between the bipolar moments $\beta_0^K(k_1, k_2; \nu')$ defined in the LAB frame and the PDDCSs $(1/\sigma)d\sigma_{kq}/d\omega_t$ defined in the CM frame.³³ Hence, the PDDCSs are determined from the observed composite Doppler profiles $D_0^K(k_1, k_2; \nu)$. In addition to the recoil speed and scattering angle distributions in the CM frame, the angular distribution function $P(\theta_r, \phi_r)$ is then calculated from Eq. (7).

C. The fitting procedure

The set of PDDCSs is determined self-consistently from the least-squares fitting. The experimental composite Doppler profiles $D_0^K(k_1, k; \nu)$ are fit with the linear combination of the basis functions $B_0^K(k_1, k; \nu; f_T, \cos \theta_t; q)$,

$$\begin{aligned} D_0^K(k_1, k; \nu) &= \sum_{f_T} \sum_{\cos \theta_t} \sum_q c_{kq}(f_T, \cos \theta_t) \\ &\times B_0^K(k_1, k; \nu; f_T, \cos \theta_t; q). \end{aligned} \quad (9)$$

The basis functions $B_0^K(k_1, k; \nu; f_T, \cos \theta_t; q)$ represent the contribution of the q component of the PDDCSs to $D_0^K(k_1, k; \nu)$ resolved into a specific CM scattering angle θ_t and the fraction of the available energy (excluding the internal energy of the observed product), released into the product CM translational energy, f_T . The set of coefficients $c_{kq}(f_T, \cos \theta_t)$ determined by the fitting procedure represents the PDDCSs for each f_T . In the present analysis, the f_T region ranging from 0.0 to 1.0 was divided into 7 bins while the region of $\cos \theta_t$ ranging from -1.0 to 1.0 was divided into 10 bins, i.e., $70 (= 7 \times 10)$ basis functions were used for this fitting.

For the preparation of the basis functions, the knowledge of the recoil velocity distribution and translational anisotropy of $O(^1D)$ produced from the 193 nm photodissociation of N_2O is required. Felder *et al.* using an angle-resolved time-of-flight mass spectroscopy method reported the recoil speed-angular distribution of $O(^1D)$ generated from the photodissociation of N_2O at 193 nm.⁴⁰ In order to consider all the possible collisions, the velocity distribution of $O(^1D)$ was convoluted with isotropic thermal motions of the precursor N_2O and the reactant H_2O , and the angle between the velocity vectors of the reactants $O(^1D)$ and H_2O . Isotropic thermal motions of N_2O and H_2O molecules were assumed to be represented by the Maxwell-Boltzmann distributions at 300 K. The angular dependence of the signal integrated over the recoil speed distribution was described by a single anisotropy parameter of $\beta_{\text{photo}} = 0.48$.⁴⁰ However, Suzuki *et al.* recently showed a recoil speed dependence of β_{photo} for $O(^1D)$ produced from the photodissociation of N_2O at 205 nm by using a two-dimensional imaging technique.⁴¹ They described the observed recoil energy and angular distribution as the superposition of the two Gaussian distributions; a broad one with $\beta_{\text{photo}} = 0.0$ and a relatively narrow one with $\beta_{\text{photo}} = 1.3$. In the present study, as a reasonable assumption, the observation at 205 nm by Suzuki *et al.* is adapted for the 193 nm result. We fit the translational energy distribution measured by Felder *et al.* with two components of broad and narrow Gaussian type distributions. The average $\beta_{\text{photo}} = 0.48$ was reproduced by setting $\beta_{\text{photo}} = 0.0$ for the broad component and $\beta_{\text{photo}} = 1.03$ for the narrow component. In practice, from the comparison between the single and double β_{photo} distributions, it was found that the details of the recoil speed dependence of the translational anisotropy of the atomic reagent does not affect the product DCS and f_T distribution significantly.

The fitting procedure with nonorthogonal basis functions as attempted in this study is one of the notorious problems giving an unphysical solution in numerical analysis. In such a situation, a least-squares fitting typically gives an over-structured DCS as the best solution. To obtain a physically

reasonable DCS with a smooth shape, we used singular value decomposition fitting⁴² giving a set of orthogonal basis functions from a set of original nonorthogonal functions. Then, the angular resolution of the DCS obtained with this algorithm becomes not so sensitive to the number of the basis functions. Furthermore, a maximum-entropy method⁴² was utilized for eliminating physically meaningless solutions such as negative values of $c_{00}(f_T, \cos \theta_i)$ representing the product f_T -resolved DCS which should not be negative. The analysis was carried out with the assumption that the reaction probability and the set of PDDCSs do not depend significantly on the initial translational energy of the reactants (the collision energy).

IV. RESULTS AND DISCUSSION

A. Scalar properties

As described in Sec. I, even with the isotopically unlabeled reagents used in this study, the observed products $\text{OH}(v'=2)$ can be exclusively assigned to the new OH since the population of the old ^{18}OH in $v'=2$ was far below the detection level in isotopically labeled studies.^{5,6} The vibrational state distribution of the old ^{18}OH was reported to be 94% in $v'=0$ and 6% in $v'=1$.⁶ Concerning the new OH, the vibrational state distribution was reported to be 39: 29: 32 for $v'=0;1;\geq 2$. These figures indicate that the $(v_{\text{new}}, v_{\text{old}}) = (2, 0)$ channel is dominant compared with the $(2, 1)$ channel. Even with the extreme assumption that the new OHs in $v_{\text{new}}=0$ and 1 levels are exclusively paired with $v_{\text{old}}=0$ level, the 32% occurrence of the new $\text{OH}(v'=2)$ would be distributed into $(2, 0)$ channel with 26% and $(2, 1)$ channel with 6%. Therefore, at least more than 80% of the new $\text{OH}(v'=2)$ is paired with the old $\text{OH}(v'=0)$. This fact means that the translational energy distribution of the new $\text{OH}(v'=2)$ in a specific rotational level almost corresponds to the rotational state distribution of the old OH (the coproduct) in $v'=0$.

Figure 2 shows the observed composite Doppler profiles for the $\text{OH}(^2\Pi_{3/2}, v'=2, j'=5.5)$ generated in the $\text{O}(^1D) + \text{H}_2\text{O}$ reaction, $D_0^0(0,0;v)$ and $D_0^2(2,0;v)$, reflecting the LAB speed distribution and recoil anisotropy, respectively. The smooth solid lines in Fig. 2 represent the least-squares fitting for the experimental data. The f_T distribution determined by the least-squares fitting is displayed in Fig. 3(a). From the f_T distribution, it is estimated that about 60% of the available energy excluding the internal energy of the observed new $\text{OH}(v'=2, j'=5.5)$ are channeled into the product CM translational energy and the residual 40% are channeled into the internal energy of the coproduct old OH. Such dominance of the energy partitioning into translational degrees of freedom can be recognized from the comparison between the observed f_T distribution and statistical one calculated by only considering the energy conservation as shown in Fig. 3(a).

The internal energy distribution of the old OH paired with the observed new $\text{OH}(v'=2)$ could be estimated by convoluting the $(1-f_T)$ distribution with the collision energy distribution. The approximate rotational state distribution of the old $\text{OH}(v'=0)$ obtained by neglecting the occur-

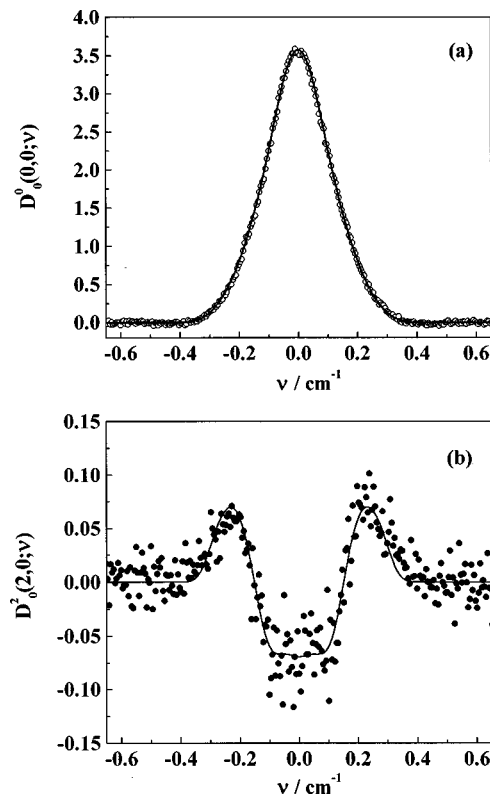


FIG. 2. Observed composite Doppler profiles for the product $\text{OH}(^2\Pi_{3/2}, v'=2, j'=5.5)$ (a) $D_0^0(0,0;v)$ (○) and (b) $D_0^2(2,0;v)$ (●). The smooth solid lines are the best fits in the Doppler analysis.

rence of the $(v_{\text{new}}=2, v_{\text{old}}=1)$ channel as discussed at the beginning of this section is displayed in Fig. 3(b). Tanaka *et al.* reported the internal state distributions of the new and old OH products generated from the isotopically labeled reaction (1) with the same $\text{O}(^1D)$ source as in the present study.^{10,11} The Boltzmann rotational state distribution with $T_{\text{rot}} = 2600$ K for the old $^{18}\text{OH}(v'=0)$ determined by Tanaka *et al.* is also displayed in Fig. 3(b). The rotational state distribution of the old OH in the $(2, 0)$ channel obtained in the present study is, though slightly cold, quite close to the result reported in Ref. 10.

Tanaka *et al.* measured the overall rotational state distribution of the old $^{18}\text{OH}(v'=0)$ whose sister fragments of the new OH could span all the energetically accessible vibrational levels, $v'=0-3$. Although we specified the rovibronic level $v'=2$ and $j'=5.5$ for the new OH, the rotational distributions of the old $\text{OH}(v'=0)$ deduced in both cases are quite similar. That is, the rotational state distribution of the old OH depends very weakly on the rovibrational state of the new OH in this reaction. This trend is partly due to the smallness of the energy distributed to the old OH; the average rotational energy of the old $^{18}\text{OH}(v'=0)$ of 22 kJ/mol corresponds to only 14% of the total available energy.

B. Vector properties

1. Differential cross section

The product total DCS averaged over the whole f_T region determined by the least-squares fitting procedure is displayed in Fig. 4. The DCS has substantial intensities over a

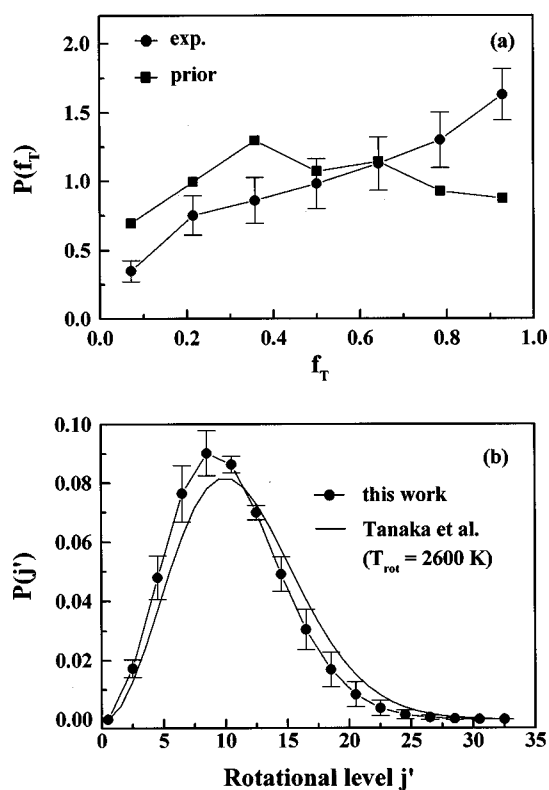


FIG. 3. (a) f_T distribution of the product $\text{OH}(^2\Pi_{3/2}, v'=2, j'=5.5)$ (●). A prior distribution (■). (b) Rotational state distribution of the old $\text{OH}(v'=0)$ paired with the observed new $\text{OH}(^2\Pi_{3/2}, v'=2, j'=5.5)$ (●). The solid line is the overall rotational state distribution of the $^{18}\text{OH}(v'=0)$ generated from the isotopically labeled reaction of the $^{16}\text{O}(^1D)$ with H_2 ^{18}O (Ref. 10). The error bars correspond to $\pm 1\sigma$.

wide angular range with slightly preferred backward scattering. This result cannot be predicted either from the direct abstraction mechanism yielding backward peaking or the direct stripping mechanism yielding forward peaking. The nearly isotropic DCS most probably indicates that the reaction proceeds via an insertion pathway involving the formation of an intermediate HOOH complex which survives for a time comparable to or longer than its rotational period.

Another possible explanation for the observed nearly isotropic DCS is a combination of rebound and stripping

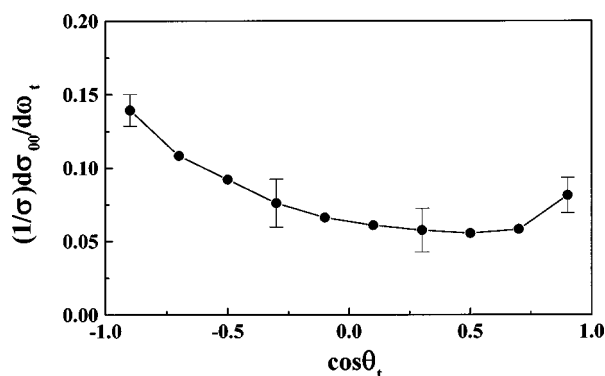


FIG. 4. Total differential cross sections averaged over the whole f_T region for the product $\text{OH}(^2\Pi_{3/2}, v'=2, j'=5.5)$. The error bars correspond to $\pm 1\sigma$.

pathways. However, this cannot be the case in the present reaction based on the following consideration. In extracting the DCS, we can obtain information about the dependence of the DCS on the product recoil energy. The evaluated recoil energy distributions of the products scattered in the forward and backward hemispheres did not show any significant difference between them. If the direct stripping and abstraction pathways actually occur, the recoil energy distributions for the forward scattering corresponding to the stripping pathway should be different from that for the backward scattering corresponding to the rebound pathway. Thus, the absence of significant dependence of the recoil energy distribution on the scattering angles suggests the insertion pathway involving a complex which survives for a rotational period. Furthermore, as will be described in the following subsection, the observed angular momentum polarization did not also largely depend on the scattering angles. This result also supports the insertion pathway rather than a combination of stripping and abstraction pathways since the dynamical constraints arising from an abstraction pathway is expected to be weaker than an insertion pathway and leads to a weaker angular momentum polarization for the backward component.

The nearly isotropic DCS obtained in this work seems to disagree with the anisotropic CM scattering angle distribution emphasized in the previous Doppler study performed by King *et al.*⁷ However, they measured only the composite Doppler profile corresponding to $D_0^0(0,0; \nu)$ and analyzed the data simply with a single scattering angle without allowing for the spread of angular distribution in the scattering. They obtained the representative scattering angles of 60° – 86° for the new OH products in various rovibrational levels. These values do not largely deviate from 90° that corresponds to the average scattering angle in the completely isotropic scattering. Therefore, such representative values of scattering angles previously reported by King *et al.* can be considered to suggest a nearly isotropic scattering angle distribution with a slight preference in the forward hemisphere rather than an anisotropic scattering. In this sense, these two results do not seriously disagree with each other.

The nearly isotropic DCS described above implies that the reaction proceeds via a long-lived intermediate complex which is generally expected to yield statistical internal energy distributions. However, it is reported in many researches^{1–11} that this reaction yields extremely unequal internal energy partitioning between the two OH products. These conflicting findings suggest that the redistribution of the available energy among the internal modes of the intermediate complex does not occur on a time scale comparable to the rotational period of the complex. Similar nonstatistical energy distributions for the complex-mode reactions involving long-lived complexes have been found in the reactions $\text{O}(^1D) + \text{CH}_4 \rightarrow \text{OH} + \text{CH}_3$ (Refs. 43, 44) and $\text{H}(^2S) + \text{CO}_2 \rightarrow \text{OH} + \text{CO}$.^{45–49} The real time pump–probe experiments by utilizing ultrafast lasers were carried out for these reactions and the results indicated that each reaction involved a long-lived complex with lifetime of picosecond order [3 ps for the $\text{O}(^1D) + \text{CH}_4$ reaction and 0.5–5 ps for the $\text{H}(^2S) + \text{CO}_2$ reaction]. However, as opposed to a traditional expectation for complex-mode reactions, the energy distributions for these

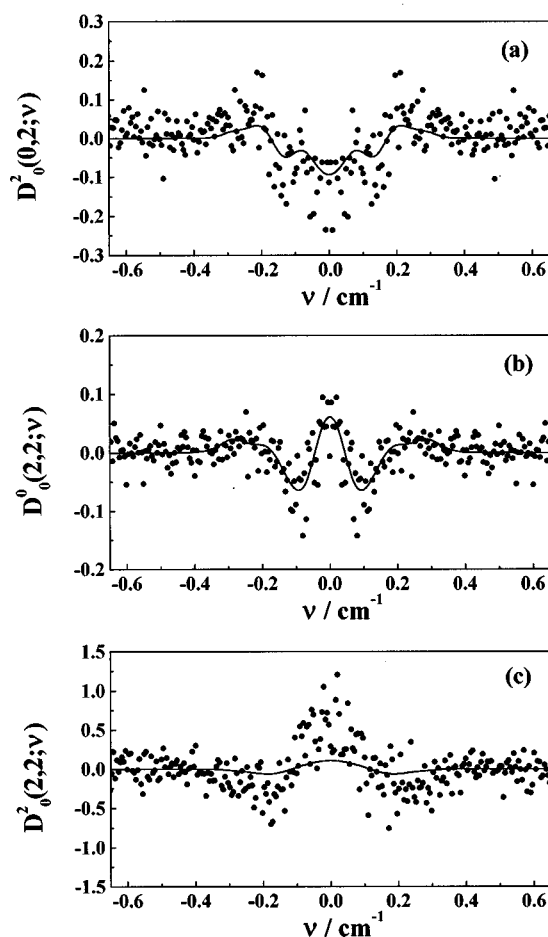


FIG. 5. Observed composite Doppler profiles of the product $\text{OH}(^2\Pi_{3/2}, v' = 2, j' = 5.5)$. (●) (a) $D_0^2(0,2;\nu)$, (b) $D_0^0(2,2;\nu)$, and (c) $D_0^2(2,2;\nu)$. The smooth solid lines are the best fits in the Doppler analysis.

reactions were found to apparently deviate from the statistical predictions in both reactions. These results imply that the absolute value of lifetime of the collisional complex is not the unique essential factor to determine the degree of energy redistribution. The rotational period of the collisional HOOH complex can be roughly estimated to be about 0.5 ps by using the rotational constants of the H_2O_2 molecule⁵⁰ and the initial orbital angular momentum ($\approx 40\hbar$) of the reactants. Thus, a nearly isotropic DCS obtained in this work suggest that the lifetime of a collisional HOOH complex is larger than 0.5 ps. Since this lifetime is shorter than those of the other two reactions described above, the nonstatistical energy distributions¹⁻¹¹ for the reaction of $\text{O}(^1D) + \text{H}_2\text{O} \rightarrow \text{OH} + \text{OH}$ is not unexpected.

2. Rotational angular momentum polarization

Figure 5 shows the set of composite Doppler profiles $D_0^2(0,2;\nu)$, $D_0^0(2,2;\nu)$, and $D_0^2(2,2;\nu)$, reflecting the rotational angular momentum polarization for the product $\text{OH}(^2\Pi_{3/2}, v' = 2, j' = 5.5)$. The smooth solid lines in Fig. 5 represent the least-squares fitting for the composite Doppler profiles. The fitting gives the polarization-dependent differential cross sections (PDDCSs) shown in Fig. 6. Further, the angular distribution function $P(\theta_r, \phi_r)$ of the product rota-

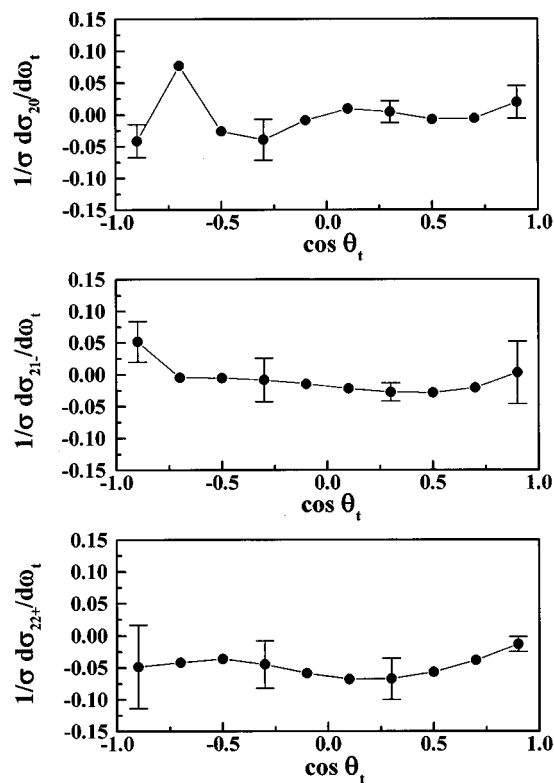


FIG. 6. The set of polarization-dependent differential cross sections for the product $\text{OH}(^2\Pi_{3/2}, v' = 2, j' = 5.5)$. (a) $(1/\sigma)d\sigma_{20}/d\omega_t$, (b) $(1/\sigma)d\sigma_{21-}/d\omega_t$, and (c) $(1/\sigma)d\sigma_{22+}/d\omega_t$. The error bars correspond to $\pm 1\sigma$.

tional angular momentum vector, \mathbf{j}' , averaged over the whole range of scattering angle derived by using Eq. (7) is shown in Fig. 7. As noted in Sec. III, θ_r is the angle between \mathbf{k} and \mathbf{j}' , while ϕ_r is the dihedral angle between the $\mathbf{k}\mathbf{k}'$ and $\mathbf{k}\mathbf{j}'$ planes. Thus, the two peaks near $(\theta_r, \phi_r) = (90^\circ, 90^\circ)$ and $(90^\circ, 270^\circ)$ imply that \mathbf{j}' is predominantly polarized perpendicular to the $\mathbf{k}\mathbf{k}'$ plane (i.e., collision plane). This preference for \mathbf{j}' perpendicular to the collision plane can be explained from a primary contribution of the bending motion of the H-O-O moiety in the HOOH collisional complex to the product rotation. This tendency for the product rotational angular momentum polarization has been recently found in the

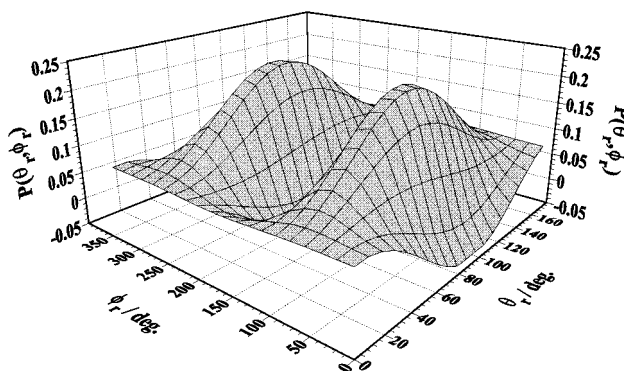


FIG. 7. Polar plots of the $P(\theta_r, \phi_r)$ representing the angular distribution of the rotational angular momentum vector of the product $\text{OH}(^2\Pi_{3/2}, v' = 2, j' = 5.5)$.

analogous reaction of $O(^1D)$ with H_2 ,¹⁸ which has been considered to proceed via an insertion pathway involving the formation of highly vibrationally excited H_2O .

The angular correlation of \mathbf{j}' perpendicular to the \mathbf{kk}' plane derived in this bimolecular reaction makes a clear contrast to the parallel $\mathbf{v}'-\mathbf{j}'$ correlation reported in the photodissociation studies of HOOH molecules.⁵¹⁻⁵³ The equilibrium position of the torsional angle is the main difference in the potential energy surfaces of HOOH molecules between the electronically ground and excited states. Hence the Franck-Condon excitation from the ground state to the excited states is followed by the torsional motion giving a parallel $\mathbf{v}'-\mathbf{j}'$ correlation to the OH photofragments. In contrast to such a specific condition in the HOOH photodissociation process, the insertion of the $O(^1D)$ atom into the OH bond of the H_2O reagent in the bimolecular reaction will give rise to the significant excitation of the stretching and bending motions of the newly formed H-O-O moiety in addition to the excitation of the torsional motion. Furthermore, the torsional angle dependence of the potential energy in the ground state⁵⁴ is much weaker than those in the excited states.⁵⁵ Therefore, the clear difference in the angular correlation between the bimolecular reaction and photodissociation of the HOOH system would be reasonably understood.

As recognized from the relatively flat behavior of each PDDCS displayed in Fig. 6, the OH products scattered in the forward and backward hemispheres have almost the same rotational angular momentum polarization; \mathbf{j}' is perpendicular to the collision plane. It suggests that irrespective of the product scattering directions, the reaction is dominated by the same mechanism, i.e., an insertion process involving a HOOH complex with a lifetime comparable to the rotational period.

As briefly mentioned in the Sec. II, in the present study, the product rotational angular momentum polarization for the two Λ -doublet states (A' and A'') was not measured separately and the analysis was performed by assuming the same angular momentum polarization for these Λ -doublet states. Since the recent studies have shown the different rotational angular momentum polarization for the Λ -doublet states in several bimolecular reactions,^{14,18,20,23} we will demonstrate the validity of such an assumption by utilizing the difference Doppler profile which is only dependent on the rotational angular momentum polarization. The difference between the profiles measured in the LIF excitation-detection geometries III and I_a corresponds to $D_0^2(0,2;\nu) + (c_4/c_1)D_0^2(2,2;\nu)$, where c_i is the difference between the multipliers b_i for these two geometries and the ratio c_4/c_1 is independent of the probed rotational branches. A close similarity between such profiles obtained for the rotational transitions $R_1(5.5)$ for A' and $Q_1(5.5)$ for A'' displayed in Fig. 8 indicates the small difference in the product rotational angular momentum polarization between the Λ -doublet states in this reaction. To the contrary, $D_0^2(0,2;\nu) + (c_4/c_1)D_0^2(2,2;\nu)$ will be apparently different between the A' and A'' states in the reactions showing the different angular momentum polarization for the Λ -doublet states, judging from the composite Doppler profiles $D_0^2(0,2;\nu)$ and $D_0^2(2,2;\nu)$ displayed in the studies for these reactions.^{14,18,20} Therefore, the approximation of an

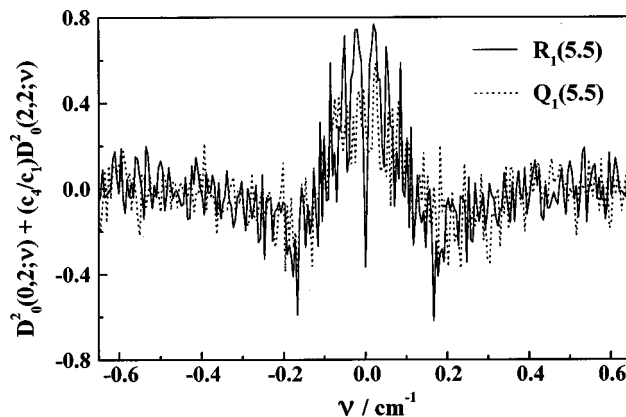


FIG. 8. Composite Doppler profiles corresponding to $D_0^2(0,2;\nu) + (c_4/c_1)D_0^2(2,2;\nu)$ for the rotational transitions of $R_1(5.5)$ and $Q_1(5.5)$. The coefficients c_i are defined in the text.

equal rotational angular momentum polarization for the two Λ -doublet states, adopted in this study, is confirmed.

C. Kinematic consideration

Combining the scalar and vector properties obtained in this study, we discuss the correlation between the two rotational angular momentum vectors of the OH products in terms of kinematic consideration. The conservation of the total angular momentum \mathbf{J} in this reaction will be satisfied as follows:

$$\mathbf{J} = \mathbf{L} + \mathbf{J}_O + \mathbf{J}_{H_2O} = \mathbf{L}' + \mathbf{j}'_1 + \mathbf{j}'_2, \quad (10)$$

where \mathbf{J}_O is the electronic orbital angular momentum of the atomic reagent $O(^1D)$ and \mathbf{J}_{H_2O} and \mathbf{j}'_i ($i=1,2$) are the rotational angular momentum vectors of the reactant H_2O and the two OH products, respectively. The orbital angular momentum vectors, \mathbf{L} and \mathbf{L}' are defined for the reactants and products, respectively. The value of J_O equals $2\hbar$ and the average value of J_{H_2O} is estimated to be $4\hbar$ at 300 K. The average value of L is estimated to be about $40\hbar$ for the average impact parameter of 1.0 \AA expected from the reaction rate constant⁵⁶ ($k = 2.0 \times 10^{-10} \text{ cm}^3 \text{ molecule}^{-1} \text{ s}^{-1}$). As shown in Fig. 9, the average value of the product CM translational energy ($\approx 45 \text{ kJ/mol}$) is close to that of the initial reagent CM translational energy, i.e., the collision energy ($\approx 39 \text{ kJ/mol}$). Thus, assuming that the impact parameter of the products is almost equal to that of the reactants, the average value of L' is estimated to be about $43\hbar$. While the rotational angular momentum of the observed new OH is $j'_1 = 5.5\hbar$, the average rotational angular momentum of the coproduct old OH is estimated to be about $j'_2 = 10.5\hbar$ from the rotational state distribution shown in Fig. 3(b).

The total angular momentum vector \mathbf{J} can be considered to be close to the initial orbital angular momentum vector \mathbf{L} since the magnitude of $\mathbf{J}_O + \mathbf{J}_{H_2O}$ estimated to be $2-6\hbar$ is much smaller than that of \mathbf{L} ($\approx 40\hbar$). Consequently, the angular momentum conservation could be approximated as $\mathbf{L} = \mathbf{L}' + \mathbf{j}'_1 + \mathbf{j}'_2$. As described in the preceding subsection, the preference of spatial correlation of \mathbf{j}'_1 perpendicular to the

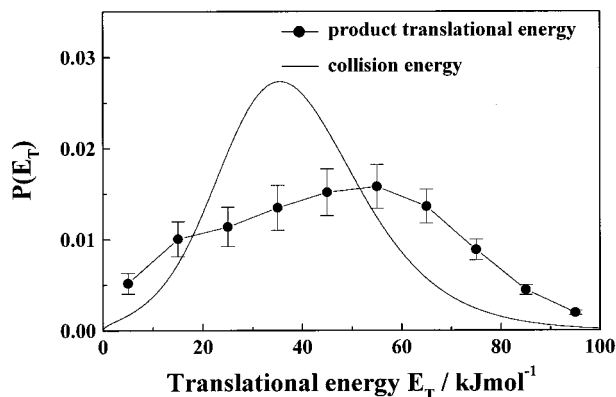


FIG. 9. Product CM translational energy (E_T) distribution. (●) The solid line is the initial translational energy (the collision energy) distribution. The error bars represent $\pm 1\sigma$.

\mathbf{kk}' plane was observed in the whole range of the angle between \mathbf{k} and \mathbf{k}' . To satisfy the conservation law and the preferential spatial correlation of $\mathbf{j}' \perp \mathbf{kk}'$ plane over the whole scattering angles at the same time, the angle between \mathbf{j}'_1 and \mathbf{j}'_2 is required to be larger than at least 90° from a simple consideration of the correlations among the set of vectors. Such a weak correlation arises from the main contribution of concerted HOOH bending motion to the torque force which rotates the product OH molecules.

V. SUMMARY

The stereodynamics of the vibrational channel generating the OH($v'=2$) in the reaction $\text{O}(^1D) + \text{H}_2\text{O} \rightarrow \text{OH} + \text{OH}$ has been investigated by observing the product state-selected differential cross section and rotational angular momentum polarization. We have observed a nearly isotropic scattering angle distribution and the preference for the perpendicular direction of the rotational angular momentum vector to the collision plane. These results indicate the formation of a HOOH collisional complex with a lifetime comparable to the rotational period and a primary contribution of the bending motion of the HOOH complex to the product rotation. The extremely asymmetrical energy partitioning between the two OH fragments, therefore, suggests that the redistribution of the available energy does not occur on a time scale comparable to the rotational period of the complex.

¹J. E. Butler, L. D. Talley, G. K. Smith, and M. C. Lin, *J. Chem. Phys.* **74**, 4501 (1981).

²K.-H. Gericke, F. J. Comes, and R. D. Levine, *J. Chem. Phys.* **74**, 6106 (1981).

³F. J. Comes, K.-H. Gericke, and J. Manz, *J. Chem. Phys.* **75**, 2853 (1981).

⁴W. A. Guillory, K.-H. Gericke, and F. J. Comes, *J. Chem. Phys.* **78**, 5993 (1983).

⁵C. B. Cleveland and J. R. Wiesenfeld, *J. Chem. Phys.* **96**, 248 (1992).

⁶D. G. Sauder, J. C. Stephenson, D. S. King, and M. P. Casassa, *J. Chem. Phys.* **97**, 952 (1992).

⁷D. S. King, D. G. Sauder, and M. P. Casassa, *J. Chem. Phys.* **97**, 5919 (1992).

⁸M. P. Casassa, D. G. Sauder, and D. S. King, *Proc. SPIE* **1858**, 256 (1993).

⁹D. S. King, D. G. Sauder, and M. P. Casassa, *J. Chem. Phys.* **100**, 4200 (1994).

¹⁰N. Tanaka, M. Takayanagi, and I. Hanazaki, *Chem. Phys. Lett.* **254**, 40 (1996).

¹¹N. Tanaka, U. Nagashima, M. Takayanagi, H. L. Kim, and I. Hanazaki, *J. Phys. Chem. A* **101**, 507 (1997).

¹²M. Brouard, S. P. Duxon, P. A. Enriquez, R. Sayos, and J. P. Simons, *J. Phys. Chem.* **95**, 8169 (1991).

¹³M. Brouard, S. P. Duxon, P. A. Enriquez, and J. P. Simons, *J. Chem. Phys.* **97**, 7414 (1992).

¹⁴M. Brouard, H. M. Lambert, J. Short, and J. P. Simons, *J. Phys. Chem.* **99**, 13571 (1995).

¹⁵M. Brouard, H. M. Lambert, C. L. Russell, J. Short, and J. P. Simons, *Faraday Discuss.* **102**, 179 (1995).

¹⁶A. J. Alexander, M. Brouard, S. P. Rayner, and J. P. Simons, *Chem. Phys.* **207**, 215 (1996).

¹⁷A. J. Alexander, F. J. Aoiz, M. Brouard, I. Burak, Y. Fujimura, J. Short, and J. P. Simons, *Chem. Phys. Lett.* **262**, 589 (1996).

¹⁸A. J. Alexander, F. J. Aoiz, L. Bañares, M. Brouard, J. Short, and J. P. Simons, *J. Phys. Chem. A* **101**, 7544 (1997).

¹⁹A. J. Alexander, D. A. Blunt, M. Brouard, J. P. Simons, F. J. Aoiz, L. Bañares, Y. Fujimura, and M. Tsubouchi, *Faraday Discuss.* **108**, 375 (1997).

²⁰M. Brouard, H. M. Lambert, S. P. Rayner, and J. P. Simons, *Mol. Phys.* **89**, 403 (1996).

²¹M. Brouard, I. Burak, G. A. J. Markillie, K. McGrath, and C. Vallance, *Chem. Phys. Lett.* **281**, 97 (1997).

²²M. Brouard, I. Burak, S. D. Gatenby, and G. A. J. Markillie, *Chem. Phys. Lett.* **287**, 682 (1998).

²³H. L. Kim, M. A. Wickramaaratchi, X. Zheng, and G. E. Hall, *J. Chem. Phys.* **101**, 2033 (1994).

²⁴R. Fei, X. S. Zheng, and G. E. Hall, *J. Phys. Chem. A* **101**, 2541 (1997).

²⁵W. R. Simpson, A. J. Orr-Ewing, T. P. Rakitzis, S. A. Kandel, and R. N. Zare, *J. Chem. Phys.* **103**, 7299 (1995).

²⁶W. R. Simpson, T. P. Rakitzis, S. A. Kandel, A. J. Orr-Ewing, and R. N. Zare, *J. Chem. Phys.* **103**, 7313 (1995).

²⁷A. J. Orr-Ewing, W. R. Simpson, T. P. Rakitzis, S. A. Kandel, and R. N. Zare, *J. Chem. Phys.* **106**, 5961 (1997).

²⁸T. P. Rakitzis, S. A. Kandel, and R. N. Zare, *J. Chem. Phys.* **107**, 9382 (1997).

²⁹T. P. Rakitzis, S. A. Kandel, T. Lev-On, and R. N. Zare, *J. Chem. Phys.* **107**, 9392 (1997).

³⁰F. Green, G. Hancock, and A. J. Orr-Ewing, *Faraday Discuss. Chem. Soc.* **91**, 79 (1991).

³¹M. L. Costen, G. Hancock, A. J. Orr-Ewing, and D. Summerfield, *J. Chem. Phys.* **100**, 2754 (1994).

³²F. J. Aoiz, M. Brouard, P. A. Enriquez, and R. Sayos, *J. Chem. Soc., Faraday Trans.* **89**, 1427 (1993).

³³F. J. Aoiz, M. Brouard, and P. A. Enriquez, *J. Chem. Phys.* **105**, 4964 (1996).

³⁴A. U. Grunewald, K.-H. Gericke, and F. J. Comes, *Chem. Phys. Lett.* **133**, 501 (1987).

³⁵C. B. Cleveland and J. R. Wiesenfeld, *Chem. Phys. Lett.* **144**, 479 (1988).

³⁶R. N. Dixon, *J. Chem. Phys.* **85**, 1866 (1986).

³⁷M. P. Docker, *Chem. Phys.* **135**, 405 (1989).

³⁸R. N. Zare, *Angular Momentum* (Wiley-Interscience, New York, 1988).

³⁹N. E. Shafer-Ray, A. J. Orr-Ewing, and R. N. Zare, *J. Phys. Chem.* **99**, 7591 (1995).

⁴⁰P. Felder, B.-M. Haas, and J. R. Huber, *Chem. Phys. Lett.* **186**, 177 (1991).

⁴¹T. Suzuki, H. Katayanagi, Y. Mo, and K. Tonokura, *Chem. Phys. Lett.* **256**, 90 (1996).

⁴²W. H. Press, B. P. Flannery, S. A. Teukolsky, and W. T. Vetterling, *Numerical Recipes in C*, 2nd ed. (Cambridge University Press, Cambridge, 1992).

⁴³C. R. Park and J. R. Wiesenfeld, *J. Chem. Phys.* **95**, 8166 (1991).

⁴⁴R. D. van Zee and J. C. Stephenson, *J. Chem. Phys.* **102**, 6946 (1995).

⁴⁵K. Kleinermanns, E. Linnebach, and Wolfrum, *J. Phys. Chem.* **89**, 2525 (1985).

⁴⁶G. Hoffmann, Y. Chen, H. Iams, and D. Oh, *J. Chem. Soc., Faraday Trans. 2* **85**, 1292 (1989).

⁴⁷N. F. Scherer, L. R. Khundkar, R. B. Bernstein, and A. H. Zewail, *J. Chem. Phys.* **87**, 1451 (1987).

⁴⁸N. F. Scherer, C. Sipes, R. B. Bernstein, and A. H. Zewail, *J. Chem. Phys.* **92**, 5239 (1990).

- ⁴⁹S. I. Ionov, G. A. Brucker, C. Jaques, L. Valachovic, and C. Wittig, *J. Chem. Phys.* **99**, 6553 (1993).
- ⁵⁰W. C. Oelfke and W. Gordy, *J. Chem. Phys.* **51**, 5336 (1969).
- ⁵¹K.-H. Gericke, S. Klee, F. J. Comes, and R. N. Dixon, *J. Chem. Phys.* **85**, 4463 (1986).
- ⁵²A. U. Grunewald, K.-H. Gericke, and F. J. Comes, *J. Chem. Phys.* **89**, 345 (1988).
- ⁵³M. P. Docker, A. Hodgson, and J. P. Simons, *Chem. Phys. Lett.* **128**, 264 (1986).
- ⁵⁴R. H. Hunt, R. A. Leacock, C. W. Peters, and K. T. Hecht, *J. Chem. Phys.* **42**, 1931 (1965).
- ⁵⁵R. Schinke, *Photodissociation Dynamics* (Cambridge University Press, Cambridge, 1993), p. 237.
- ⁵⁶K.-H. Gericke and F. J. Comes, *Chem. Phys. Lett.* **81**, 218 (1981).